Tropical Cyclone Inner-Core Kinetic Energy Evolution

Katherine S. Maclay*
CIRA/CSU, Fort Collins, Colorado 80523

Mark DeMaria
NOAA/NESDIS, Fort Collins, Colorado 80523

and

Thomas H. Vonder Haar
CIRA/CSU, Fort Collins, Colorado 80523

Submitted to
Monthly Weather Review
May 2007
Revised October 2007

*Corresponding Author
Katherine S. Maclay
CIRA/Colorado State University
Fort Collins, CO 80523-1375
maclay@cira.colostate.edu

Abstract

Tropical cyclone (TC) destructive potential is highly dependent on the distribution of the surface wind-field. To gain a better understanding of wind structure evolution, TC 0-200 km wind-fields from aircraft reconnaissance flight-level data are used to calculate the low-level area-integrated kinetic energy (KE). The integrated KE depends on both the maximum winds and wind structure. To isolate the structure evolution, the average relationship between KE and intensity is first determined. Then the deviations of the KE from the mean intensity relationship are calculated. These KE deviations reveal cases of significant structural change, and, for convenience, are referred to as measurements of storm size (storms with greater (less) KE for their given intensity are considered large (small)). It is established that TCs generally either intensify and do not grow, or weaken or maintain intensity and grow.

Statistical testing is used to identify conditions that are significantly different for growing versus non-growing storms in each intensification regime. Results suggest two primary types of growth processes: (1) secondary eyewall formation and eyewall replacement cycles, an internally dominated process; and (2) external forcing from the synoptic environment. One of the most significant environmental forcing is the vertical shear. Under light shear, TCs intensify but do not grow. Under moderate shear, they intensify less but grow more, and under very high shear they do not intensify or grow.

As a supplement to this study, a new TC classification system based on KE and intensity is presented as a complement to the Saffir-Simpson hurricane scale.

1. Introduction

Surface wind structure is a significant component of tropical cyclone (TC) destructive potential. For a large compared to a small storm of equal intensity not only will the wind damage be greater, but such a storm will also generate a larger storm surge. Storm surge is a very serious threat to coastal regions often causing greater damage than the winds (AMS, 1993). This was dramatically demonstrated by Hurricane Katrina (2005) which caused unprecedented storm surge damage to portions of Louisiana and Mississippi yet was rated only as a category 3 on the Saffir-Simpson hurricane scale (SSHS) at landfall.

TC size can vary greatly as is well illustrated by Hurricane's Charley (2004) and Wilma (2005). Both began as small-sized storms which intensified rapidly to major hurricane intensity. However, while Charley remained small throughout its evolution, Wilma experience substantial structural growth. At their respective Florida landfalls, Charley had a radius of maximum wind (RMW) of ~3 nautical miles (5.6 km) and an intensity of 64 ms^{-1}, and Wilma had a RMW of ~30 nautical miles (55.6 km) with an intensity of 54 ms^{-1} (Fig. 1). These storms, while unique in their own right, are not anomalous with respect to their structural changes.

TC intensity has consistently been measured by either maximum sustained wind or minimum central pressure. Overall size has been determined from parameters such as radius of outer closed isobar or radius of gale-force winds, while inner-core size is traditionally given by the eye diameter and RMW. Strength has been measured and defined in a great variety of ways, but is generally considered a measure of the areal extent of some defined wind speed.

In this study the wind structure is determined from 0-200 km wind-fields of TCs from 1995-2005, derived from aircraft flight-level data. Intensity is defined as the maximum wind speed (ms^{-1}) from objective analyses of flight-level data (unless otherwise specified). The wind structure parameter is the low-level area-integrated kinetic energy (KE). This integrated KE depends on both storm intensity and wind structure. To isolate the wind structure component, the KEs for the entire data set are first plotted versus intensity revealing a general trend of mean KE compared to intensity. The KE deviations from the mean KE/maximum wind relationship are then used as a measure of the wind structure. For convenience, the KE deviations are referred to as a measure of storm size (storms with greater (less) KE for their given intensity are considered large (small)).

The KE deviation parameter is probably more closely related to what has been called "strength" in previous studies (e.g. Merrill 1984). However, strength is also commonly used as a synonym for intensity, so that terminology was not used here. The KE deviation measure of storm size is correlated with the more traditional measure of storm size as measured by the radius of gale-force winds (R34). To quantify this relationship, the values of R34 for the total aircraft analysis sample were obtained from the NHC best-track for cases since 2004, and from the NHC advisories prior to 2004 (NHC did not create best-track radii until 2004). A correlation between KE deviation values and similarly calculated R34 deviation values give a correlation coefficient of 0.6, indicating a weak, but non-negligible relationship between the KE measure of size used in this study and the more traditional size measure. All references to size and growth in this study will be with respect to the KE deviations. So, a storm is considered growing if

its KE deviations increase with time and not growing if the deviations decrease. These KE deviations are then used to identify growing and non-growing cases.

Previous studies focused on the relationship between TC intensity and size or strength. Such studies have shown that typically inner-core intensity change precedes change in the storm outer-core winds (Weatherford and Gray 1988a-b (hereafter, W-G); Merrill 1984; Croxford and Barnes 2002). Kimball and Mulekar (2004) observed that weakening storms tend to be large, intense, and highly organized as they are often more mature, whereas intensifying storms, often early in their lifecycle, are generally small and less intense. Recurvature and extratropical transition, a common occurrence in Atlantic TC (Hart and Evans 2001), have been found to affect TC size and intensity by generally decreasing intensity and increasing size (Sinclair 2002; Jones et al 2003).

Internal dynamics and synoptic forcing have been suggested as key factors in determining TC size (Cocks and Gray 2002) and intensity (Wang and Wu 2004). The model and theory based studies of Challa and Pfeffer (1980), Shapiro and Willoughby (1982), and Holland and Merrill (1984) provide some useful insights into the possible mechanisms for TC intensity and size change. Cumulatively, they suggest that upper and lower-level forcing via heat and momentum sources may be instrumental in TC size change. To further investigate these theories as well as determine other mechanisms for growth, a statistical analysis of our KE cases was performed, as described below.

The individual cases are sorted into six groups defined by the storm's state of intensification and size change. GOES infrared data for each group are examined to determine if there are convective differences between the groups. Microwave satellite data are also examined for some cases to better identify the eyewall structure. The

environmental conditions most significant for each group are analyzed using NCEP reanalysis fields. Special emphasis is given to the anomalous cases where a storm intensifies and grows, or weakens and does not grow.

As an offshoot of this research, a new hurricane scale based on integrated KE and intensity is proposed. The scale is developed as a complement to the SSHS and has the benefit of incorporating storm size. The KE scale and SSHS are compared by looking at all U.S. landfalling hurricanes from 1995-2005.

2. Data Sources

The primary data set for this study is the objectively analyzed aircraft reconnaissance flight-level data, which is used to calculate KE, as described in Section 3. A variety of auxiliary data sets are used to analyze storm attributes and conditions. Satellite data includes Geostationary Operational Environmental Satellite (GOES) infrared measurements, and the Special Sensor Microwave/Imager (SSM/I) and Special Sensor Microwave Imager/Sounder (SSMIS) microwave imagery. The National Centers for Environmental Prediction (NCEP) reanalysis data (Kistler et al 2001; Toth et al 1997) provides storm synoptic environmental conditions. Finally, assorted integrated storm and storm environment variables from the Statistical Hurricane Intensity Prediction Scheme (SHIPS) model predictors, GOES infrared data, and the aircraft reconnaissance data provide a description of a variety of attributes of each storm and its environment.

The 0-200 km wind-fields of Atlantic and Eastern Pacific TCs from 1995-2005 on a cylindrical grid (Δr = 4 km, $\Delta\theta$ = 22.5º) are determined from an objective analysis of the U.S. Air Force Reserve aircraft reconnaissance data as described by Mueller et al (2006). The 0-200 km radial domain is chosen to match the standard length of the flight

legs for the aircraft reconnaissance flights. To better capture the time evolution of the KE, the objective analysis used data composited over 6-hr intervals instead of the 12-hr intervals used by Mueller et al. The 124 storms for this study yield a total of 1244 flight-level wind-field analyses. The maximum flight-level winds from the objective analyses are also determined to investigate the relationships between intensity and size. Furthermore, variables to estimate the eye and storm sizes, respectively, are derived from the aircraft reconnaissance data. These variables are the radius of maximum symmetric tangential wind (RMSTW) and the tangential wind gradient outside the RMW (TWG).

The convective profiles and inner-core convection is investigated using 4 km resolution, storm-centered, digital GOES infrared (IR) satellite imagery (Kossin 2002). The azimuthally averaged, radial profile data extends from 0-500 km from storm-center and includes both the brightness temperatures (T_b) and the azimuthal standard deviations of the T_b at each radius, which is a measure of the convective asymmetry. Additionally, the GOES IR data are used to derive a variable to measure the inner-core convection. The variable (CONV) is the percent area in the 50-200 km radial band with T_b below -40˚C.

Imagery from the Special Sensor Microwave/Imager (SSM/I) 85 GHz and Special Sensor Microwave Imager/Sounder (SSMIS) 91 GHz horizontally polarized channels are used to identify secondary eyewall formation and eyewall replacement cycles in selected storms in Section 4. This imagery was retrieved from the NRL Monterey Marine Meteorology Division TC page: http://www.nrlmry.navy.mil/tc_pages/tc_home.html.

Variables related to the location and synoptic scale environment are acquired from the Statistical Hurricane Intensity Prediction Scheme (SHIPS) predictor variables (DeMaria et al 2005). These variables provide integrated measures of the storm thermodynamic, dynamic and internal conditions. The latitude (LAT), longitude (LON), sea surface temperature (SST), ocean heat content (OHC), magnitude of the deep shear (200-800 km radial average) (SHR), environmental 850 hPa vorticity (0-1000 km average) (VORT), and the 150 hPa temperature (T150), which gives an estimate of the tropopause height, provide information about the storm environment. The 100-600 km average 200 hPa relative eddy momentum flux convergence variable (REFC) is a good indicator of trough interactions (DeMaria et al 1993; Holland and Merrill 1984; Molinari and Vollaro 1989). The storm latitude and longitude were obtain from the NHC best-track and were utilized to calculate storm speed (SPD) and direction[1].

From the datasets described above, a broad selection of integrated variables encompassing information about the storm and storm environment were statistically analyzed to determine their relative importance in TC size change. A subset of these were found to be significantly related to size changes, which are listed in Table 1 by variable name, description, and units and scaling.

In addition to the integrated synoptic variables listed in Table 1, some of the basic synoptic fields from the NCEP reanalysis data were also examined. These include the upper (200 hPa) and lower (850 hPa) level horizontal wind-fields, the 850-200 hPa shear, and the 700 hPa temperature advection fields on 31˚ by 41˚ latitude/longitude, storm-centered grids.

[1] The direction variable revealed no statistically significant information and is therefore not presented.

3. Kinetic Energy Climatology and Hurricane Scale

As discussed in previous sections, the KE of the wind-field is likely an important factor in determining TC related destruction. This section will 1) describe a method to estimate KE from winds measured during routine reconnaissance of Atlantic and Eastern Pacific TCs, 2) describe the climatology of this KE calculation, 3) show how estimated KE is related to TC destruction, and 4) compare it to the SSHS.

To estimate KE from a single level some assumptions are necessary. First, consider the storm to be a thin disk within a constant radius and depth interval. The total KE is found by integrating the kinetic energy for a single air parcel over the volume of the disk:

$$KE = \int_{z_1}^{z_2} \int_0^{2\pi} \int_0^R \frac{1}{2} \rho (u^2 + v^2) r dr d\theta dz , \tag{1}$$

where u is radial wind, v is tangential wind, ρ is air density, r is radius, θ is azimuth, and z is height. The aircraft reconnaissance flight-level winds are assumed to be representative of the storm structure over a 1 km depth and are usually available out to a 200 km radial distance from storm-center. A constant density is assumed since the variation in air density within this volume is small. Therefore, the KE equation becomes:

$$KE = \frac{\rho_o \Delta z}{2} \int_0^{2\pi} \int_0^R (u^2 + v^2) r dr d\theta \tag{2}$$

where ρ_o is assigned a value of 0.9 kgm^{-3} (a typical air density at 700 hPa, the standard flight-level for hurricane reconnaissance flights). Using (2), KE is calculated for all analyses in the data set.

To determine how storm energy evolves during intensification, the KEs (J) are plotted versus the maximum analyzed winds (ms^{-1}) in Fig. 2. From the basic definition of

kinetic energy one would expect a storm's kinetic energy to increase with the square of the maximum wind. However, the integrated KE also depends on the wind distribution, so it would not necessarily be proportional to the square of the maximum wind. A best-fit applied to the data reveals a power series relationship:

$$KE = 3 * 10^{13} (V_{\max})^{1.872} \quad . \tag{3}$$

The variance explained, R^2, for this best-fit is 82%. Thus, KE increases with nearly the square of the maximum winds. It should be noted that the mean KE-intensity relationship does not describe the evolution of KE for individual storms and there is considerable variability in KE for a given intensity. The KE evolution through the lifecycle of individual storms is investigated more thoroughly in Section 4.

The highly active TC seasons of 2004 and 2005 and the devastation caused to Louisiana and Mississippi by Hurricane Katrina have sparked increased concern over the effectiveness of the SSHS in alerting the public accurately to a storm's potential danger. Several studies such as Kantha (2006) and Powell and Reinhold (2007) have suggested replacing the SSHS with improved scales. Kantha proposes a set of dynamic-based, continuous scales, for intensity and wind damage potential, similar to that used for earthquakes. It gives better accuracy by incorporating size into the scaling and retains a separate measure for intensity, which would be useful for small, intense storms. These calculations for the wind damage potential use the cube of the maximum wind, which, in practice, might be somewhat inaccurate due to the underlying uncertainties in the ability to estimate maximum wind (Brown and Franklin 2004). Also, a continuous and highly nonlinear scale would be valuable for sophisticated users, but might be problematic for conveying information to the general public. Powell and Reinhold proposed wind and

storm surge destructive potential scales based on integrated kinetic energy (IKE). Their IKE is calculated quite similarly to the KE in this study, but over a larger area (8x8º grid) using the H*Wind (Powell et al. 1998) analysis fields as opposed to the aircraft reconnaissance flight-level winds. Using area-integrated kinetic energy to estimate storm destructive potential takes into account both intensity and size. The SSHS only takes into account intensity. Incorporating size should provide further insight into potential storm damage by severe winds, intense rain, and storm surge. Much of the beauty and success of the SSHS is in its simplicity. In an effort to preserve the established usefulness of the SSHS yet account for aspects of size, the KE from this study is used to form a classification to complement the SSHS. This KE scale is designed to be used in conjunction with the SSHS for ease of implementation.

To illustrate the potential for a new scale, a system of six categories is defined ranging from 0 to 5, where category 0 represents tropical storms on the SSHS. The percentages of storms corresponding to each SSHS category are determined from the 1947-2004 NHC best-track data. The thresholds for the KE hurricane scale categories are chosen by applying these same percentages to the KE climatology data set. Table 2 outlines the SSHS categories, their corresponding historical distributions, and the analogous KE hurricane scale categories.

To compare these scales, consider the 1995-2005 U.S. landfalling hurricanes. Table 3 shows, for each storm, the date and time of the objective analysis closest to the storm's landfall time, time difference between the analysis and the actual landfall, intensity from the analysis, official NHC intensity at landfall, SSHS category, the KE calculated from the analysis, and the KE scale category. Storms with two landfalls, such

as Hurricane Katrina, which crossed Florida before making its final landfall in Louisiana and Mississippi, are indicated by (1) for the first landfall and (2) for the second.

The KE values for the analysis closest in time to landfall for each storm are plotted against the official NHC intensities (ms^{-1}) in Fig. 3. The vertical dotted lines mark thresholds for the SSHS categories and the horizontal dotted lines are thresholds for the KE hurricane scale categories. Observe first the data points for Hurricane's Katrina (2005) and Ivan (2004). On the SSHS Katrina made landfall on the Louisiana/Mississippi border as a category 3, however, the KE scale measures the storm as an impressive category 5. Similarly, Ivan was nearly a KE category 5 at landfall, and it too was a SSHS category 3. Katrina caused an estimated $75 billion (Knabb et al 2006) and Ivan an estimated $14.2 billion (Franklin et al 2006) in damage. These were the two most costly storms in the U.S. from 1995-2005, yet they were not the most intense to make U.S. landfall for this period. However, for both of these storms much of the damage was a result of storm surge. Thus, the KE scale appears to provide additional information about a hurricane's potential for damage that is not available solely from intensity.

The main weakness of the KE and intensity scales is that they do not accurately represent the destructive potential of small, intense storms. Hurricane Charley (2004), which caused an estimated $14 billion in damage, is a good example. At its first landfall in Punta Gorda, Florida the storm measured a category 4 on the SSHS, but it was a KE category 0. At its second landfall in Myrtle Beach, South Carolina it had weakened to a SSHS category 1, yet increased to a KE category 1. At first landfall the storm was an extremely intense, compact system. While it contained very strong winds, they were

confined to within 6 nautical miles (11.1 km) of the storm-center based on the flight-level winds. Such a small RMW makes it impossible to adequately resolve the high wind features near the eyewall even in the reconnaissance data (which has 4 km resolution). At the second landfall it had weakened with respect to its maximum sustained winds, but had become a larger system with fairly high winds covering a greater area resulting in an increased KE. The most significant damage occurred during initial landfall and was caused by extreme winds rather than storm surge, of which there was a minimal amount. Powell and Reinhold attempt to account for these small, intense storms by weighting storms with ≥ 55 ms^{-1} more heavily in their scale, yet they still noted similar weaknesses in representing the destructive potential of small, intense storms such as Charley. A better understanding of wind destructive potential is likely necessary to adjust these scales to account for such storms. An alternate approach is to simply use the SSHS and KE scales in conjunction as both provide valuable information about storm destructive potential.

4. KE Evolution

While the overall evolution in KE with respect to intensity is generally defined by the power series curve (3), individual storms rarely evolve in this manner. This is best illustrated by the time evolution of individual storm KE deviations (KE') from the mean curve as a function of intensity. The KE' are calculated as the difference between the measured and expected KE for the storm's intensity from (3). A zero value in KE' indicates the storm has the expected KE for its intensity and lies upon the mean curve described by (3) and shown in Fig. 2. As described previously, increasing KE' implies storm growth and decreasing KE' implies the storm is not growing relative to its intensity

evolution. The KE' evolution is examined for all storms with at least three associated aircraft analyses, of which there are 97 cases.

a. "Horizontal Question Mark" Evolution

Extensive review of the KE' evolution plots reveal some common characteristics. TCs more commonly intensify and decrease in KE' (i.e., do not grow) or decrease in intensity and increase in KE' (i.e., grow). The opposites occur less frequently. In fact, a unique evolution in intensity and structure is apparent, which will be referred to as the "Horizontal Question Mark" evolution for simplicity. Examples of this can be seen in Fig. 4 which shows the time evolution of KE' versus V_{max} plots for six TCs. Storms that had reconnaissance data extending through the greater part of the storm's evolution, such as Hurricane's Katrina and Wilma (2005), showed this pattern most commonly. This evolution suggests that as a storm begins to intensify there is often a modest decrease in KE', but as a stage of more rapid intensification is reached the KE' decreases substantially. Once reaching peak intensity and weakening begins the KE' often increases. These findings comply with previous studies by W-G and Merrill (1984) which suggested TCs generally do not intensify and grow simultaneously, as well as Kimball and Mulekar's (2004) findings that, generally, weakening storms are large and intensifying storms small.

b. Eyewall Replacement Cycles (ERCs)

Examining the KE' vs. V_{max} plots in combination with microwave and IR for several major hurricanes revealed that secondary eyewall formation and eyewall replacement cycles (ERCs) (Willoughby et al 1982) are often associated with nearly discrete KE' changes. As the secondary eyewall begins to dominate its larger size results

in a KE' increase even though the V_{max} has often weakened during this process. The new, larger eye may then become more organized, intensify, and contract completing the ERC. Thus, an intensity increase and KE' decrease is seen.

Hurricane Wilma (2005) had a dramatic ERC early in the storm's lifetime. Fig. 5 shows the KE' evolution with respect to intensity for Wilma with corresponding microwave imagery overlain (points A-D). Wilma formed in the Caribbean (Fig. 5-A) and very quickly intensified into an extremely small, intense TC (Fig. 5-B). Its tiny eye then became encompassed by a much larger secondary eyewall. The small eye broke down leaving the larger eye in its place (Fig. 5-C) which then proceeded to organize and intensify (Fig. 5-D). The storm's development, as shown in the microwave imagery, is clearly evident in the KE' and intensity evolution. As the storm developed to its peak intensity the KE' decreased (A-B). During the ERC the intensity decreased, but the KE' increased (B-C) as the larger eye formed. Finally, as the new eye began to contract the storm experienced moderate intensification and a KE' decrease(C-D).

Wilma's ERC illustrates a discrete growth process common to strong TCs. During the ERC the storm initially loses intensity as the inner eyewall breaks down and is replaced by an existing secondary eyewall. The new eye may contract as the storm re-intensifies, but generally remains larger than the previous eye. This is a primary mechanism for storm growth, and was also seen in several other storms including Ivan (2004) and Floyd (1999).

c. Intensity Change/Size Change Regimes

To confirm the prevalence of these evolutional tendencies and facilitate further analysis of storm structural evolution, time tendencies of intensity and KE' are

calculated. The time tendencies are calculated using centered time differences, with one-sided differences at the beginning and end of each time series. The reconnaissance analysis times are unequally spaced in time so the tendencies are normalized to a 24-hr period, and are denoted by ΔV_{max} and $\Delta KE'$. Also, $\Delta KE'$ and ΔV_{max} values are only used for analyses at least three hours, but less than 24 hours, apart. This restriction avoids unrealistic values for the 24-hr intensification or growth when the aircraft reconnaissance analyses are too close or far apart. Eastern Pacific storms are excluded from this portion of the analysis due to the basins limited availability of aircraft data. This should not affect the results as this eliminates only a few storms leaving 91 storms and a total of 1123 analyses for this portion of the study.

The ΔV_{max} and $\Delta KE'$ values are sorted by intensity change, and three groups are defined: the lower third represents weakening storms (W), the upper third intensifying storms (I), and the middle third storms approximately maintaining intensity (M). The weakening, maintaining and intensifying groups are split into growing (i.e., positive $\Delta KE'$) and non-growing (i.e., negative $\Delta KE'$) groups, represented by G and NG, respectively. Table 4 shows that weakening storms are more often growing, and intensifying storms are more often not growing. This supports not only previous studies, but also provides a quantitative measure of the preliminary investigation of the KE'/V_{max} evolution shown in Fig. 4. ('Horizontal Question Mark'). The growing, weakening (GW) and non-growing, intensifying (NGI) cases in Table 4 correspond to negative slopes in the V_{max}, KE' phase-space diagram in Fig. 4, and the non-growing, weakening (NGW) and growing, intensifying (GI) cases correspond to positive slopes. The maintaining

intensity cases (GM, NGM) have small slopes. In the large sample, 50.4% of the cases have negative slopes, while only 16.3% are positively sloped.

5. Conditions Associated With Structure Changes

A climatology of TC growth with respect to intensification suggests that generally weakening storms grow and intensifying storms do not grow. While these observations are interesting, they are not all that enlightening. Using the available data divided into the six groups introduced above (GW, NGW, GI, NGI, GM, and NGM), the following sections discuss mechanisms for TC growth.

a. Basic Storm and Storm Environmental Conditions

A first step is to determine characteristics and basic environmental conditions common to each of the six groups in Table 4. Utilizing the objectively analyzed reconnaissance data, GOES IR brightness temperature (T_b) profile data, and the SHIPS model data records, information about both the storm at the time of each analysis and the associated environmental conditions are retrieved and sorted into arrays based on the group classifications.

How the environmental conditions for the G versus NG storms in each intensification scenario compare is of particular interest. To determine these relationships the difference in the means of G from NG storms is calculated and is non-dimensionalized by normalizing by the standard deviations of each variable. Statistical analysis using the student's t-test is employed to determine the probability that a given variable is significantly different for G versus NG storms in each intensification regime. A 95% significance threshold isolates variables worthy of further investigation. Table 5

shows the mean value for each variable in each group. The shading indicates where the 95% significance threshold *has* been met.

While usually storms either intensify or grow, but not do both simultaneously, occasionally storms weaken and do not grow, or intensify and grow (these are termed the 'anomalous' storms). From the results shown in Table 5 some prevalent conditions are associated with anomalous structural development.

Consider GI storms in comparison to the typical NGI storms. These storms tend to be located at higher latitudes, farther west, with lower tropopause heights (warmer T150). They are positioned over lower ocean heat content waters and experience higher shear and eddy momentum flux convergence suggesting trough interaction. They have less inner-core convection, a larger radius of maximum symmetric tangential wind, and a smaller tangential wind gradient outside the RMW. The higher shear and momentum fluxes indicate that trough interaction is important for growth in intensifying storms. A numerical modeling study by Kimball and Evans (2002) showed that in idealized scenarios trough interaction results in increased TC size and strength, but decreased maximum intensity in comparison to a simply shear influenced storm. In the real atmosphere a trough may supply the extra angular momentum needed to support simultaneous intensification and growth. Also, many of the conditions normally associated with intensification (low shear, warm SST and high OHC) are less for GI cases. This suggests that in environments favorable for intensification, changes are more confined to the inner-core, and have less impact on storm size.

The second anomalous case is NGW storms. Compared to GW cases, these storms general move more quickly, are located at higher latitudes, have lower tropopause

heights, and are positioned over cooler SSTs and lower ocean heat content waters. They experience greater shear, and lower values of environmental vorticity. Less inner-core convection, a larger inner-core, and a smaller tangential wind gradient outside the RMW are also common to these storms. These characteristics are indicative of storms in a less favorable environment preventing the normal growth seen in weakening storms. Generally, those factors which contribute to growth in an intensifying storm restrict growth in weakening storms. In these cases, the conditions may be so hostile that the storm is on its way to final dissipation or extratropical transition. Keeping this in mind, greater focus will be given to GI storms from this point forward. To better understand these processes a more in depth study of the convection and synoptic environments is necessary.

b. Convective Profiles

For a better understanding of the structure of inner- and outer-core heating in the different storm types consider the GOES IR brightness temperature (T_b) and standard deviations in T_b radial profiles. High clouds from more intense convection measure as colder T_bs, so the T_b profiles reveal more information about the storm convective structure. The standard deviation in T_b provides a measure of the asymmetry of convection where higher values indicate greater convective asymmetry. It is noted that cirrus canopy from a convectively active eyewall may obscure rainband convection in the infrared imagery. However, the absence of cold cloud-top temperatures in the infrared imagery is a guarantee that there is no underlying deep convection.

Although the T_b profiles for intensifying storms do not show significant differences in their means, there are some interesting features (Fig. 6 *top*). At the storm-

center the cloud-top temperatures are nearly the same, but the T_b profiles diverge noticeably outwards through the eyewall. The NGI storms exhibit colder cloud-tops through the eyewall indicating an increased convective region. The GI storms, on the other hand, show a flatter, less convective T_b profile through the eyewall.

The profiles T_b standard deviation for intensifying storms exhibit significant differences for GI versus NGI storms (Fig. 6 *bottom*). Near the storm-center (6-10 km) NGI storms show greater convective asymmetry, but near the eyewall and extending out to the outer rainbands (30-330 km) GI storms are more convectively asymmetric. This suggests GI storms have more heating occurring outside the eyewall and extending into the rainbands than NGI storms.

c. Synoptic Environments

Using NCEP reanalysis data corresponding to each aircraft reconnaissance analysis, a composite analysis of the storm-centered horizontal wind-fields is created for pressure levels of 200, 500, 700 and 850 hPa. The magnitude of the 850-200 hPa shear vectors are calculated using the composite 200 hPa and 850 hPa horizontal winds. The 2-D wind-field and deep shear plots provide a more detailed view of the synoptic conditions associated with each storm type.

Consider first the 200 hPa, 850 hPa and deep shear fields for intensifying storms. The 200 hPa mean wind-fields for both NGI and GI (Fig. 7) storms show evidence of the upper-level anticyclone that customarily form over TCs. An upper-level trough is evident west of both the GI and NGI storms, but for GI storms it is stronger and extends farther south, which displaces the anticyclone a little farther east of the storm-center. In addition, the winds around the anticyclone are less axisymmetric for GI storms as a result

of the trough interaction. This distortion of the wind-field indicates that the trough may be importing momentum into the storm. This supports earlier findings for the 200 hPa relative eddy momentum flux convergence (REFC) variable, which measured greater 200 hPa momentum flux in GI storms (4.4 m/s/day) than in NGI storms (3.0 m/s/day).[2]

The 850 hPa wind-fields for NGI and GI (Fig. 8) storms are dominated primarily by storm flow. Weak anti-cyclonic circulations directly north of NGI storms and northwest of GI storms indicate that intensifying TCs are typically south of the North Atlantic subtropical ridge. The GI cases appear to be located in a break in the subtropical ridge.

Given the presence of a stronger upper-level trough, which has been shown to displace the upper-level anticyclone, a greater magnitude of deep vertical shear is expected for GI versus NGI storms. A contour plot of differences in the mean shear of GI from NGI storms (Fig. 9) supports this. The shear is greater northeast of GI versus NGI storms.

Weakening storms have similar 200 hPa, 850 hPa, and deep shear fields (not shown). However, the differences between GW and NGW cases are universally opposite to those of intensifying cases.

Thus there may be an optimal value of vertical shear for storm growth. For very low values, the convection is confined to the storm-center, so intensification occurs without growth (the typical case). When the shear is a little higher, as in the IG anomalous case, the convection is a little less symmetric and there is greater convection

[2] The 100-600 km average 200 hPa planetary/earth eddy momentum flux convergence variable was considered, motivated by Merrill's (1984) considerations of earth angular momentum contributions to TC size. Statistical testing determined that the differences in the variable were insignificant for growing versus non-growing storms in each intensification regime.

outside the main eyewall. These storms continue to intensify, but also grow. When the shear is too high storms do not intensify or grow (as in the anomolous WNG cases).

The 700 hPa temperature advection ($-\vec{V}\cdot\nabla T$) fields are computed using 700 hPa horizontal wind and temperature fields to determine significant differences in the baroclinic environments. Positive temperature advection values represent regions of warm air advection (WAA), and negative values cold air advection (CAA).

The 700 hPa temperature advection fields for GI storms show an interesting temperature advection dipole with strong WAA in the northeast quadrant and CAA in the northwest quadrant (Fig. 10 *right*). This dipole feature is not evident in NGI storm temperature advection fields (Fig. 10 *left*), which suggests that this highly baroclinic environment is a factor for growth in intensifying storms. A strikingly similar temperature advection dipole feature is also present for NGW storms (not shown) implying that similar baroclinic effects influence these storms. However, the effect with respect to growth is opposite for weakening storms. The dipole in Fig. 10 suggests rising motion east of the storm-center for GI cases. This result is consistent with the GOES IR standard deviation differences which showed that these storms have more asymmetric convection away from storm-center. These characteristics could be symptomatic of the initial stages of extratropical transition. Studies have shown that during extratropical transition TCs become more convectively asymmetric, experience increased translation speed, decreased intensity as well as an expansion in their wind-fields as they travel into the more highly sheared, baroclinic midlatitudes (Sinclair 2002; Klein et al 2000; Jones et al 2003). Furthermore, interactions with upper-level troughs become more likely as TCs move towards the midlatitudes. However, to better understand the causes and effects of

the temperature advection dipole feature prevalent in both anomalous storm types, further study is necessary through a complete energy budget analysis.

d. Summary of Mechanisms for Tropical Cyclone Growth

The results of statistical testing and subsequent analysis imply that there are two primary ways for storms to grow. The first is growth through secondary eyewall formation, which was identified and discussed in Section 4 as a mechanism for storm growth. The second type of growth is induced by environmental forcing. Environmental forcing can be caused by momentum flux from trough interactions, a more highly sheared environment, temperature advection, or a combination of these features. When a storm is in a stage of intensification, trough interaction may import additional momentum into the core inducing growth. The baroclinicity of the storm environment can also be a source of forcing. TC development is generally thought to require a vertically stacked (barotropic) structure. However, the formation of a more tilted (baroclinic) vertical structure may cause growth by stimulating convection via heating outside of the symmetric inner-core. This is suggested by the greater convective asymmetry in GI storms extending out from the eyewall. Vertical tilt is a likely result of shear from a trough or some other atmospheric disturbance. Shear can cause baroclinic instability, and hence, temperature advections with flow across a temperature gradient. In this situation, potential energy from the baroclinic instability might be converted into kinetic energy in the storm leading to growth.

Environmentally forced growth applies only to storms that are in an intensification stage. For weakening storms environmental forcing has a negative effect on structure. Recall the mean values of deep shear (SHR) for intensifying and weakening

storms in Table 5. The environmental shear for both GW and GI is comparable (8.4 ms^{-1} and 8.5 ms^{-1}, respectively). However, for NGW storms the shear is a notably higher 9.8 ms^{-1}. Thus moderate environmental forcing may result in storm growth; however, too much forcing can cause complete storm decay.

6. Case Studies

Having determined through statistical analysis common features and characteristics for various types of storm structural evolution, validation of these results is in order. Three storms have been chosen based upon the categorization of the analyses for each storm. These cases present examples of typical and atypical structural evolution. Time series of the storm's intensity, KE', environmental shear, and 200 hPa eddy momentum flux convergence are compared with the synoptic analysis for each storm. The shear and eddy momentum flux convergence variables are chosen as they are good indicators of possible environmental forcing.

a. Hurricane Mitch (1998)

Hurricane Mitch (1998) experienced a fairly typical structural evolution. Fig. 11 shows the time series of intensity (ms^{-1}), environmental shear (ms^{-1}), 200 hPa eddy momentum flux convergence (ms^{-1} per day), and KE' (10^6 J) for the storm, as well as the storm track from the NHC best-track data. The analyses correspond to October 23 18 UTC to October 29 12 UTC. The time series plots show that from October 23 18 UTC to October 26 12 UTC, the analyses categorize the storm as NGI, and during the period October 27 6 UTC to October 29 12 UTC, as WG. The KE' time series essentially mirrors the intensity time series illustrating the growth and non-growing pattern through the storm's intensification and weakening stages. The intensifying stage indicated by the

analyses encompasses the time shortly before the storm became a hurricane, located to the southwest of Jamaica, until it reached maximum intensity on the 26th. During this time it underwent rapid intensification. A reported symmetric, well-established upper-tropospheric outflow pattern evident in satellite imagery is suggestive of a low-shear, undisruptive synoptic environment which allowed a typical intensification process (Pasch et al 2001). On the 27th the storm passed over Swan Island, shear increased, and the storm began to weaken in intensity, a process which would continue through the 29th when it made landfall in Honduras. The minimal values of eddy momentum flux convergence indicate that it did not experience much environmental forcing. Aside from land interactions, which were likely a crucial factor in the storm's weakening stages, Mitch was in an environment well-suited to host a substantial TC.

b. Hurricane Dennis (1999)

Hurricane Dennis (1999) was an atypical storm which experienced trough interactions that appear to have enhanced the storm's structural evolution. The time series of intensity (ms^{-1}), environmental shear (ms^{-1}), 200 hPa eddy momentum flux convergence (ms^{-1} per day), and KE' (10^6 J), and the storm track are shown in Fig.12. The analyses correspond to August 25 00 UTC to August 31 12 UTC. Dennis formed August 26th in the western Atlantic at the east-southeast end of a trough and in upper-level westerly shear (Lawrence et al 2001). This environment caused convective asymmetries in the storm with a greater amount in its eastern portion, and prevented the storm's circulations from consolidating, as is normally seen in TCs, keeping the RMW fairly large throughout the storm's initial intensification. The increasing shear and eddy momentum flux convergence in the first portion of Fig. 12 were caused by the initial

trough interaction. During this period the KE' also increased indicating a growth of the wind-field. The shear decreased late on the 27th after which the storm reached its peak intensity of 46 ms^{-1} on the 28th. However, a second mid-latitude trough interaction on the 28th and 29th caused a more northward movement of the storm. During this time the RMW in the storm remained large (extending 70-85 nautical miles (129.6-157.4 km) August 29-30). This second trough interaction is evident in the time series plots of the shear and eddy momentum flux convergence. Even with increased shear and momentum flux, the storm maintained and even increased intensity, although at a fairly slow rate compared to Hurricane Mitch. Furthermore, the KE' increased as well during this period as the storm's circulation grew.

c. Hurricane Wilma (2005)

The structural evolution of Hurricane Wilma (2005) can be separated into two stages: a first stage when the structure was controlled by internally dominated processes, and a second when it was more influenced by environmental forcing. The time series of intensity (ms^{-1}), environmental shear (ms^{-1}), 200 hPa eddy momentum flux convergence (ms^{-1} per day), and KE' (10^6 J), and the storm track are shown in Fig. 13. The analyses correspond to October 17 18 UTC to October 25 00 UTC. During the first stage, while the storm was in the Caribbean, it intensified and grew through an ERC, as described in detail in Section 4. This ERC, which occurred on October 18-19, is clearly evident on the KE' and intensity time series as a large increase and moderate decrease in intensity and a corresponding large decrease and increase in KE'. As the storm traveled over the Gulf of Mexico towards and across southern Florida it continued to grow and intensify, however this development was a result of synoptic forcing. A strong mid-tropospheric

trough which steered the storm along this path also created a strongly sheared environment (Pasch et al 2006). The trough interactions during the storm's passage over the Gulf of Mexico are evident by the increasing shear and eddy momentum flux in the latter part of the time series plots. During this time, however, the storm continued to intensify and maintain and even increase a bit in size, as is demonstrated by the KE' trend. This supports the hypothesis that trough interactions and more highly sheared environments can induce growth provided that they are not so strong as to cut off the intensification process.

7. Conclusions and Future Work

The overall impact of a tropical cyclone (TC) is highly dependent upon the surface wind structure. To study this, the 0-200 km integrated kinetic energy data recorded from 1995-2005 of Atlantic and East Pacific TCs has been used to establish a climatology of TC KE. A new KE hurricane scale has been presented that shows promising results in predicting TC destructive potential when applied to U.S. landfalling hurricanes from 1995-2005. This KE scale supplements the Saffir-Simpson Hurricane Scale (SSHS) by more accurately representing the destructiveness of TCs. A study of the trends in the KE with respect to intensity and structure demonstrated that TCs either intensify and do not grow, or weaken and grow. Occasionally, however, a storm deviates from this evolution and grows in a stage of intensification or doesn't grow during a weakening stage. To better understand the factors behind growth in storms in different stages of intensity change, statistical testing determined significant differences between growing and non-growing storms for a wide range of variables. Collectively these studies provide an idea of the underlying mechanisms responsible for storm growth.

Two main types of growth mechanisms for intensifying TCs were identified. The first method was through secondary eyewall formation and subsequent ERC. During an ERC storms initially lose intensity as the inner eyewall breaks down and is replaced by an existing secondary eyewall. The new, larger eye may contract as the storm re-intensifies but generally remains larger than the previous eye. The result is an overall storm growth. The second mechanism for growth was via environmental forcing. Forcing can be caused by momentum flux from a trough interaction where flow from an approaching trough imports momentum into the storm environment and increases the wind-field. Another source of forcing could be from baroclinic effects of a sheared environment and/or temperature advection in the near storm environment. A vertically sheared environment can cause convection to be displaced to outer regions of the storm. Similarly, the advection of warm air into a storm will lead to enhanced convection in these regions. An increase in convection in the external regions of the inner-core and into the outer-core can cause an overall growth for an intensifying storm.

It is interesting to note that the conditions which create an environment most suitable for growth in an intensifying storm have the opposite effect upon the growth of a weakening storm. In absence of environmental forcing a storm will develop in a typical manner (NGI, and GW), and with moderate forcing a storm may intensify and significantly increase its wind-field (GI). However, storms cannot sustain intensity or their wind-fields if there is too much environmental forcing (NGW). Essentially, these conditions disrupt the normal structural evolution causing a storm to evolve in an atypical manner such that an intensifying storm will grow and a weakening storm will fall apart.

To gain a more substantial understanding of the causes of growth in a TC further investigations are necessary. First, a more thorough look at the convective structure using the 2-D GOES IR T_b profiles would provide a way to determine the location of convective asymmetries. This is of particular interest in studying WNG storms and IG storms, both of which have more asymmetric convection than their G/NG counterparts.

The next step is to carry out a full modeling study to better understand TC structure change. The observed KE evolution of a few specific TCs in the 1995-2005 data set representing both types of structural evolution as well as the mechanisms that may contribute to TC structural change, could be compared to WRF (Weather Research and Forecasting) model simulations of those storms. Furthermore, a complete energy budget calculation using a model study would help determine the mechanisms behind TC growth. This information could be used to develop a prediction system for storm structure change. Such a prediction system would be a valuable tool for providing more accurate warnings to those areas in danger during the TC seasons.

Acknowledgements

This research was sponsored by CIRA activities and participation in the GOES Improved Measurement Product Assurance Plan (GIMPAP) under NOAA cooperative agreement NA17RJ1. The authors thank Wayne Schubert and three anonymous reviewers for providing comments that improved this manuscript. Views, opinions, and findings in this report are those of the authors and should not be construed as an official NOAA and/or U.S. Government position, policy, or decision.

References

AMS, 1993: Policy Statement: Hurricane detection, tracking and forecasting. *Bull. Amer. Meteor. Soc.*, **74**, 1377-1380.

Brown, D., and J. Franklin, 2004: Dvorak tropical cyclone wind speed biases determined from reconnaissance-based "Best Track" data (1997-2003). *26th Conf. on Hurricanes and Tropical Meteorology*, Monterey, California, Amer. Meteor. Soc., 3D.5.

Challa, M., and R. Pfeffer, 1980: Effects of eddy fluxes of angular momentum on model hurricane development. *J. Atmos. Sci.*, **37**, 1603-1618.

Cocks, S., and W. Gray, 2002: Variability of the outer wind profiles of Western North Pacific typhoons: Classification and techniques for analysis and forecasting. *Mon. Wea. Rev.*, **130**, 1989-2005.

Croxford, M., and G. Barnes, 2002: Inner-core strength of Atlantic tropical cyclones. *Mon. Wea. Rev.*, **130**, 127-139.

DeMaria, M., J-J Baik, and J. Kaplan, 1993: Upper-level eddy angular momentum fluxes and tropical cyclone intensity change. *J. Atmos. Sci.*, **50**, 1133-1147.

DeMaria, M., M. Mainelli, L. Shay, J. Knaff, and J. Kaplan, 2005: Further improvements to the Statistical Hurricane Intensity Prediction Scheme (SHIPS). *Wea. Forecasting*, **20**, 531-543.

Franklin, J., R. Pasch, L. Avila, J. Beven, M. Lawrence, S. Stewart, and E. Blake, 2006: Atlantic hurricane season of 2004. *Mon. Wea. Rev.*, **134**, 981-1025.

Hart, R., and J. Evans, 2001: A climatology of the extratropical transition of Atlantic tropical cyclones. *J. Climate*, **14**, 546-564.

Holland, G., and R. Merrill, 1984: On the dynamics of tropical cyclone structural changes. *Quart. J. Roy. Meteor. Soc.*, **110**, 723-745.

Jones, S., P. Harr, J. Abraham, L. Bosart, P. Bowyer, J. Evans, D. Hanley, B. Hanstrum, R. Hart, F. Lalaurette, M. Sinclair, R. Smith, and C. Thorncroft, 2003: The extratropical transition of tropical cyclones: Forecast challenges, current understanding, and future directions. *Wea. Forecasting*, **18**, 1052-1092.

Kantha, L., 2006: Time to replace the Saffir-Simpson Hurricane Scale? *Eos. Trans. Amer. Geophys. Union,* **87**, 3-6.

Kimball, S., and J. Evans, 2002: Idealized numerical simulations of hurricane-trough interactions. *Mon. Wea. Rev.*, **130**, 2210-2227.

Kimball, S., and M. Mulekar, 2004: A 15-year climatology of North Atlantic tropical cyclones -- Part I: Size parameters. *J. Climate*, **17**, 3555-3575.

Kistler, R., and Coauthors, 2001: The NCEP-NCAR 50-year reanalysis: Monthly means CD-ROM and documentation. *Bull. Amer. Meteor. Soc.*, **82**, 247-267.

Klein, P., P. Harr, and R. Elsberry, 2000: Extratropical transition of Western North Pacific tropical cyclones: An overview and conceptual model of the transformation stage. *Wea. Forecasting*, **15**, 373-395.

Knabb, R., J. Rhome, and D. Brown, cited 2006: Tropical cyclone report, hurricane Katrina. [Available online at http://www.nhc.noaa.gov/pdf/TCR-AL122005_Katrina.pdf]

Kossin, J., 2002: Daily hurricane variability inferred from GOES infrared imagery. *Mon. Wea. Rev.*, **130**, 2260-2270.

Lawrence, M., L. Avila, J. Beven, J. Franklin, J. Guiney, and R. Pasch, 2001: Atlantic hurricane season of 1999. *Mon. Wea. Rev.,* **129**, 3057-3084.

Merrill, R.T., 1984: A comparison of large and small tropical cyclones. *Mon. Wea. Rev.*, **112**, 1408-1418.

Molinari, J., and D. Vollaro, 1989: External influences on hurricane intensity --Part I: Outflow layer eddy angular momentum fluxes. *J. Atmos. Sci.*, **46,** 1093-1105.

Mueller, K., M. DeMaria, J. Knaff, and T. H. Vonder Haar, 2006: Objective estimation of tropical cyclone wind structure from infrared satellite data. *Wea.Forecasting*, **21**, 990-1005.

Pasch, R., L. Avila, and J. Guiney, 2001: Atlantic hurricane season of 1998. *Mon. Wea. Rev.*, **129**, 3085-3123.

Pasch, R., E. Black, H. Cobb, and D. Roberts, cited 2006: Tropical cyclone report, hurricane Wilma. [Available online at http://www.nhc.noaa.gov/pdf/TCR-AL252005_Wilma.pdf]

Powell, M., S. Houston, L. Amat, and N. Morisseau-Leroy, 1998: The HRD real-time hurricane wind analysis system. *J. Wind Eng. Ind. Aerodyn.*, **77-78**, 53-64.

Powell, M., and T. Reinhold, 2007: Tropical cyclone destructive potential by integrated kinetic energy. *Bull. Amer. Meteor. Soc.*, **88**, 1-14.

Shapiro, L., and H. Willoughby, 1982: The response of balanced hurricanes to local sources of heat and momentum. *J. Atmos. Sci.*, **39**, 378-394.

Sinclair, M., 2002: Extratropical transition of Southwest Pacific tropical cyclones -- Part I: Climatology and mean structure changes. *Mon. Wea. Rev.,* **130**, 590-609.

Toth, Z., E. Kalnay, S. Tracton, R. Wobus, and J. Irwin, 1997: A synoptic evaluation of the NCEP ensemble. *Wea. Forecasting*, **12**, 140-153.

Wang., Y., and C.-C. Wu., 2004: Current understanding of tropical cyclone structure and intensity changes – a review. *Meteor. Atmos. Phys.*, **87**, 257-278.

Weatherford, C., and W.M. Gray, 1988-a: Typhoon structure as revealed by aircraft reconnaissance -- Part I: Data analysis and climatology. *Mon. Wea. Rev.,* **116**, 1032-1043.

Weatherford, C., and W.M. Gray, 1988-b: Typhoon structure as revealed by aircraft reconnaissance -- Part II: Structural variability. *Mon. Wea. Rev.,* **116**, 1044-1056.

Willoughby, H., J. Clos, and M. Shoreibah, 1982: Concentric eye walls, secondary wind maxima, and the evolution of the hurricane vortex. *J. Atmos. Sci.*, **39**, 395-411.

Figure Caption List

Figure 1: GOES infrared image of Hurricane's Charley (2004) (*left*) and Wilma (2005) (*right*) at the time of their respective Florida landfalls.

Figure 2: KE versus Intensity (V_{max} from the aircraft reconnaissance analyses).

Figure 3: The approximate KE versus V_{max} as reported by NHC at landfall for all U.S. landfalling hurricanes from 1995-2005.

Figure 4: Time evolution of KE' versus V_{max} for six selected storms. Note in particular the plots for hurricane's Katrina and Wilma.

Figure 5: The KE' vs. V_{max} evolution of Hurricane Wilma with relevant microwave imagery overlain to illustrate the occurrence of an eyewall replacement cycle.

Figure 6: Mean radial profiles of the GOES IR brightness temperatures *(top*) and standard deviation in brightness temperatures (*bottom*) for intensifying storms. The boxes indicate the areas where the G versus NG storm profiles showed statistically significant differences.

Figure 7: 200 hPa mean wind-fields [kts] for intensifying storms. The left-hand image shows the composite field for the non-growing storms, and the right-hand image shows the composite field for the growing storms. The cyclone symbol denotes the location of the center of the hurricane. The 'A' marks the location of the upper-level anticyclone.

Figure 8: 850 hPa mean wind-fields [kts] for intensifying storms. The left-hand image shows the composite field for the non-growing storms, and the right-hand image shows the field for the growing storms. The cyclone symbol denotes

the location of the center of the hurricane. The 'A' marks the location of the anticyclone circulation associated with the North Atlantic subtropical ridge.

Figure 9: The difference in the mean 850-200 hPa shear [ms^{-1}] fields (growing – nongrowing) for intensifying storms. The cyclone symbol denotes the location of the center of the hurricane.

Figure 10: 700 hPa mean temperature advection [Ks^{-1}] fields for intensifying, non-growing (left) and growing (right) storms. The cyclone symbol denotes the location of the center of the hurricane.

Figure 11: Time series of the intensity (ms^{-1}), environmental shear (ms^{-1}), 200 hPa eddy momentum flux convergence (ms^{-1} per day), and KE deviations (10^{16} J) from the mean curve for Hurricane Mitch (1998) (*left*); and the storm's track through its entire lifetime from NHC best-track (*right*). The time series plot corresponds to the storm's track over the Caribbean Ocean. The colors indicate the storm's intensity and the numbered data points correspond to day of the month.

Figure 12: Time series of the intensity (ms^{-1}), environmental shear (ms^{-1}), 200 hPa eddy momentum flux convergence (ms^{-1} per day), and KE deviations (10^{16} J) from the mean curve for Hurricane Dennis (1999) (*left*); and the storm's track through its entire lifetime from NHC best-track (*right*). The colors indicate the storm's intensity and the numbered data points correspond to day of the month.

Figure 13: Time series of the intensity (ms^{-1}), environmental shear (ms^{-1}), 200 hPa eddy momentum flux convergence (ms^{-1} per day), and KE deviations (10^{16} J) from

the mean curve for Hurricane Wilma (2005) (*left*); and the storm's track through its entire lifetime from NHC best-track (*right*). The colors indicate the storm's intensity and the numbered data points correspond to day of the month.

Tables and Figures

Table 1: Storm and storm environment variables used in this study

Variable Name	Description	Units and Scaling	
SST	Reynolds Sea Surface Temperature	˚C	SHIPS Model
T150	150 hPa Temperature	˚C	
LAT	Latitude	˚N	
LON	Longitude	˚W	
SHR	850-200 hPa shear magnitude	ms^{-1}	
VORT	850 hPa vorticity	sec^{-1} * 10**5	
REFC	200 hPa relative eddy momentum flux convergence	m/sec/day, 100-600 km average	
OHC	Ocean heat content derived from satellite altimetry	kJ/cm^2	
SPD	Storm speed	ms^{-1}	
CONV	% area r = 50-200 km with Brightness Temperature < -40˚C	%	GOES
RMSTW	Radius of maximum symmetric tangential wind	km	Aircraft Reconnaissance
TWG	Tangential wind gradient outside the radius of maximum wind	$100*ms^{-1}/km$	

Table 2: The SSHS and the proposed Kinetic Energy Hurricane Scale (KEHS)

Category	SSHS (V_{max}) (ms^{-1})	Percentage (%)	KEHS ($*10^{16}J$)
0	**17 – 32**	**53.0**	**< 2.84**
1	**33 – 42**	**24.4**	**2.84 – 5.35**
2	**43 – 49**	**10.9**	**5.35 – 7.09**
3	**50 – 58**	**6.5**	**7.09 – 8.56**
4	**59 – 69**	**4.2**	**8.56 – 10.0**
5	**≥ 70**	**1.1**	**> 10.0**

Table 3: Data for all U.S. landfalling hurricanes (1995-2005) at approximately the time of their respective landfall.

Storm Name	Average Analysis Time (Month/Day Hour:Min)	Time before Landfall (Hour:Min)	Analysis V_{max} (ms^{-1})	NHC V_{max} (ms^{-1})	SSHS Category	KE ($*10^{16}J$)	KEHS Category
Erin (1) '95	08/02 04:49	1:26	39.0	38.6	1	3.35	1
Erin (2) '95	08/03 14:36	1:24	43.8	38.6	1	2.52	0
Opal '95	10/04 01:28	20:32	43.2	51.4	3	4.47	1
Bertha '96	07/12 20:52	-0:52	46.4	46.3	2	4.07	1
Fran '96	09/05 21:36	2:54	54.6	51.4	3	8.83	4
Danny (1) '97	07/18 04:21	4:39	34.9	33.4	1	1.23	0
Danny (2) '97	07/19 16:01	1:59	31.1	33.4	1	1.45	0
Bonnie '98	08/27 04:57	-0:57	38.9	48.9	2	5.34	1
Earl '98	09/03 04:15	1:45	38.7	36.0	1	3.02	1
Georges (1) '98	09/25 23:12	-7:42	42.7	46.3	2	5.52	2
Georges (2) '98	09/27 21:04	14:26	41.1	46.3	2	6.03	2
Bret '99	08/22 16:23	7:37	59.9	51.4	3	3.96	1
Floyd '99	09/16 05:24	1:06	50.1	46.3	2	6.92	2
Lili '02	10/03 10:20	2:40	45.9	41.2	1	5.27	1
Claudette '03	07/15 13:54	1:36	40.6	41.2	1	2.73	0
Isabel '03	09/18 15:51	1:09	57.3	46.3	2	8.10	3
Charley (1) '04	08/13 16:53	3:52	56.4	64.3	4	2.45	0
Charley (2) '04	08/14 10:09	5:51	38.8	33.4	1	3.29	1
Gaston '04	08/28 21:19	16:41	28.2	33.4	1	1.50	0
Frances '04	09/05 05:11	-0:41	48.6	46.3	2	7.02	2
Ivan '04	09/15 19:46	11:04	63.3	54.0	3	9.99	4
Jeanne '04	09/26 05:01	-0:59	48.5	54.0	3	7.02	2
Dennis '05	07/10 20:21	-0:51	55.5	54.0	3	4.04	1
Katrina (1) '05	08/25 20:47	1:43	35.5	36.0	1	1.99	0
Katrina (2) '05	08/29 14:44	0:01	62.5	54.0	3	11.35	5
Rita '05	09/23 21:07	10:33	57.5	53.6	3	9.56	4
Wilma '05	10/24 04:18	6:12	59.2	54.0	4	8.76	4

Table 4: The percentage of analyses associated with each intensification/growth regime

	Weakening	**Maintaining**	**Intensifying**
Non-Growing	7.3%	13.9%	24.3%
Growing	26.1%	19.4%	9.0%

Table 5: Mean values for the storm/storm environment variables are shown in this table. The shaded cells indicate values that showed a 95% statistically significant difference.

	Weakening		Intensifying		Maintaining	
	NGW	**GW**	**NGI**	**GI**	**NGM**	**GM**
LAT	27	23.4	21.7	25.7	25.6	24.4
LON	76.7	74.5	74.7	78.8	72.8	75.3
SST	28.1	28.5	28.8	28.6	28.1	28.7
OHC	40.4	52.8	63.2	54.2	44.1	54.9
T150	-65.2	-65.7	-66.3	-65.5	-65.6	-65.8
SHR	9.8	8.4	7.6	8.5	9.2	7.6
VORT	23.8	34.7	40.1	44.2	29.5	25.5
REFC	3.0	3.5	3.0	4.4	3.3	3.5
SPD	3.6	4.3	4.2	4.0	4.3	3.8
CONV	52.8	67.4	73.9	65.3	62.6	66.7
RMSTW	91.0	60.1	58.7	81.8	77.1	81.7
TWG	-9.4	-22.2	-22.1	-13.3	-14.4	-15.2

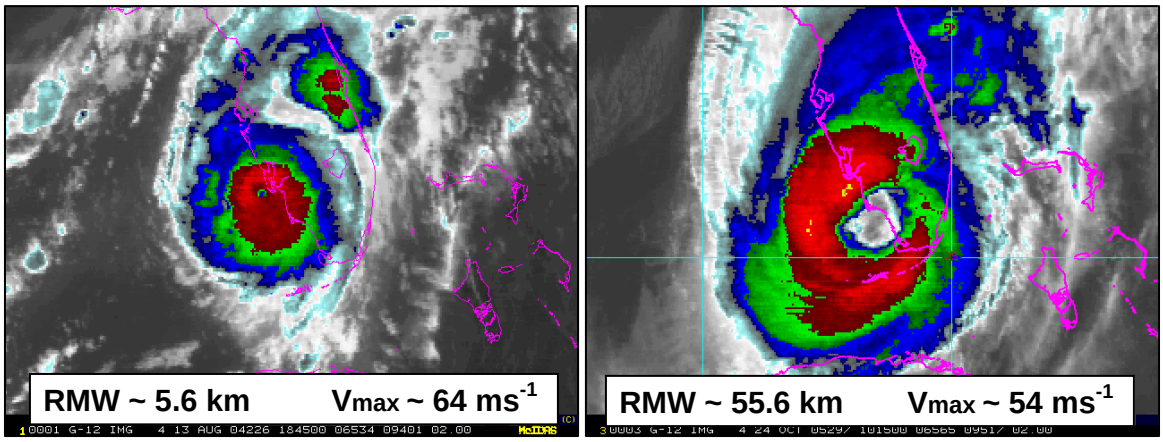

Figure 1: GOES infrared image of Hurricane's Charley (2004) (*left*) and Wilma (2005) (*right*) at the time of their respective Florida landfalls.

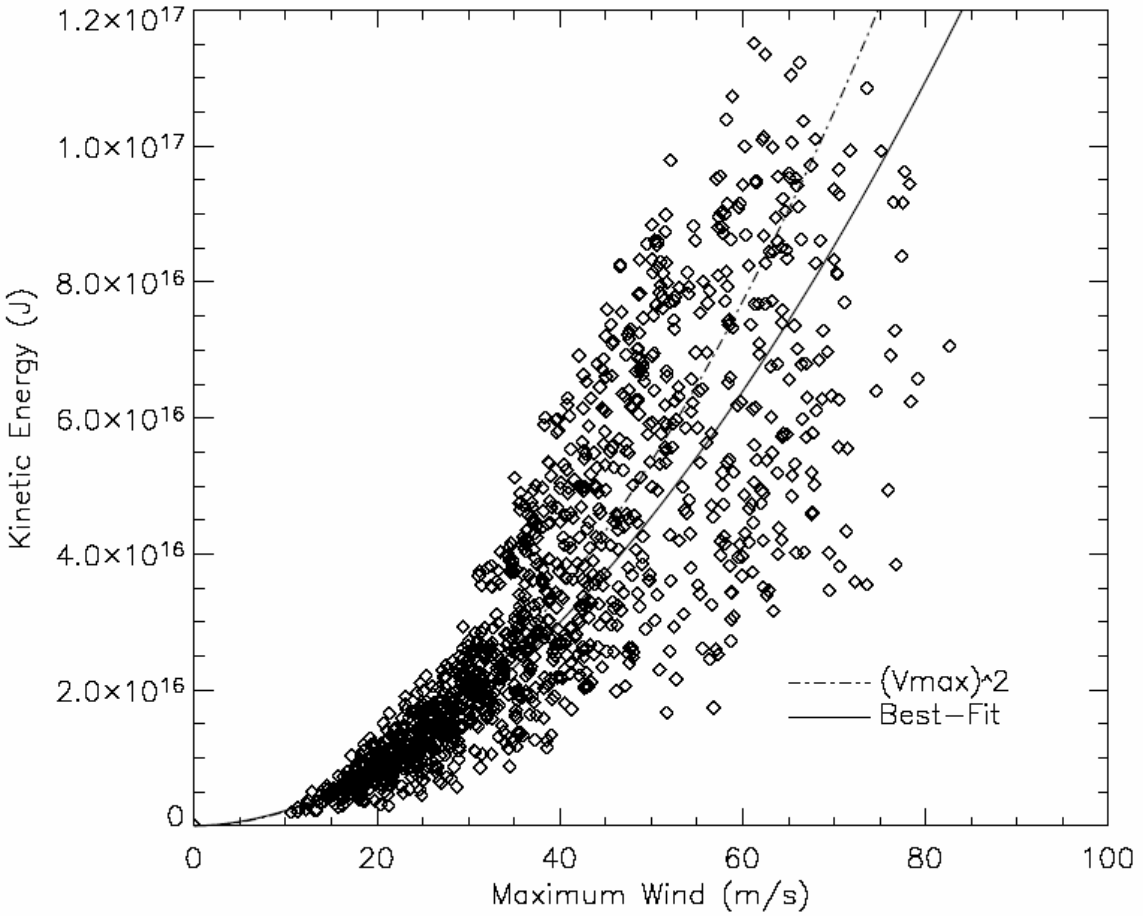

Figure 2: KE versus Intensity (V_{max} from the aircraft reconnaissance analyses).

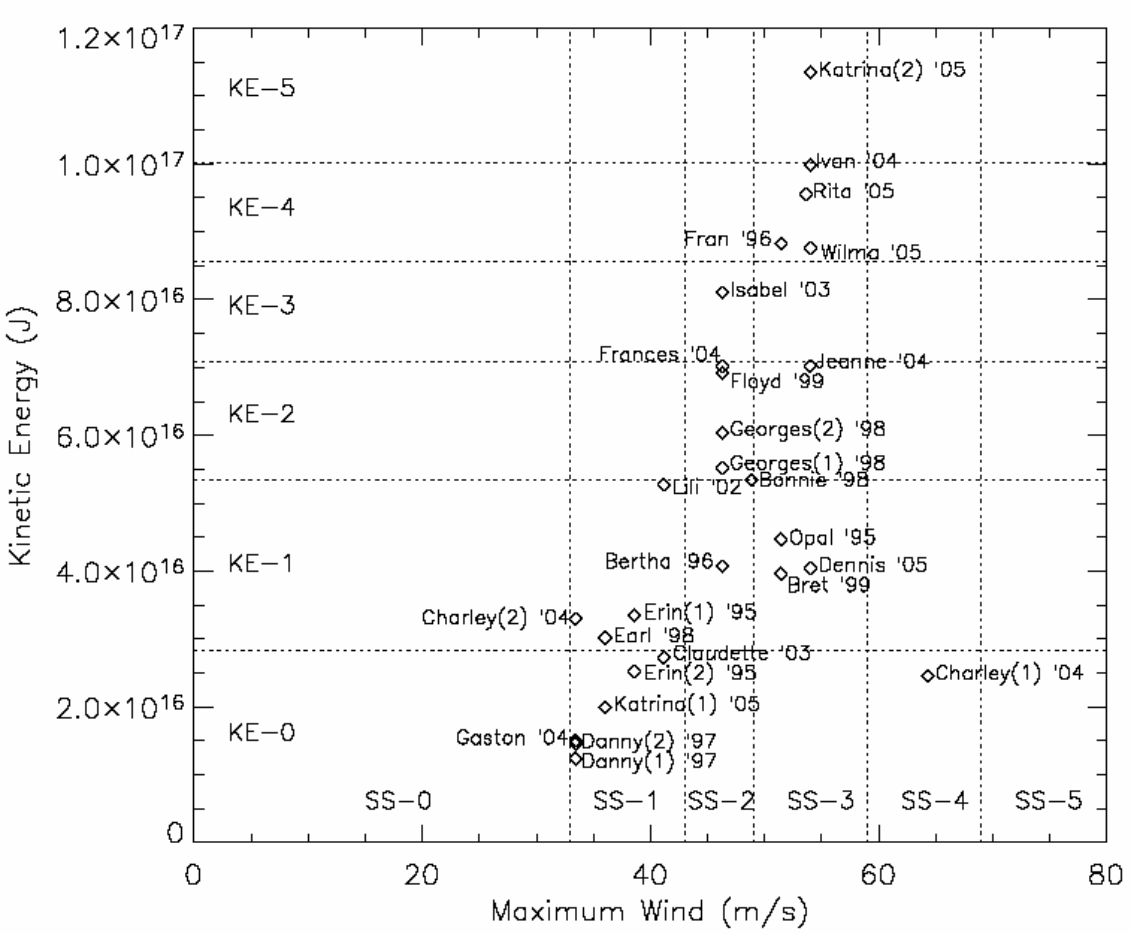

Figure 3: The approximate KE versus V_{max} as reported by NHC at landfall for all U.S. landfalling hurricanes from 1995-2005.

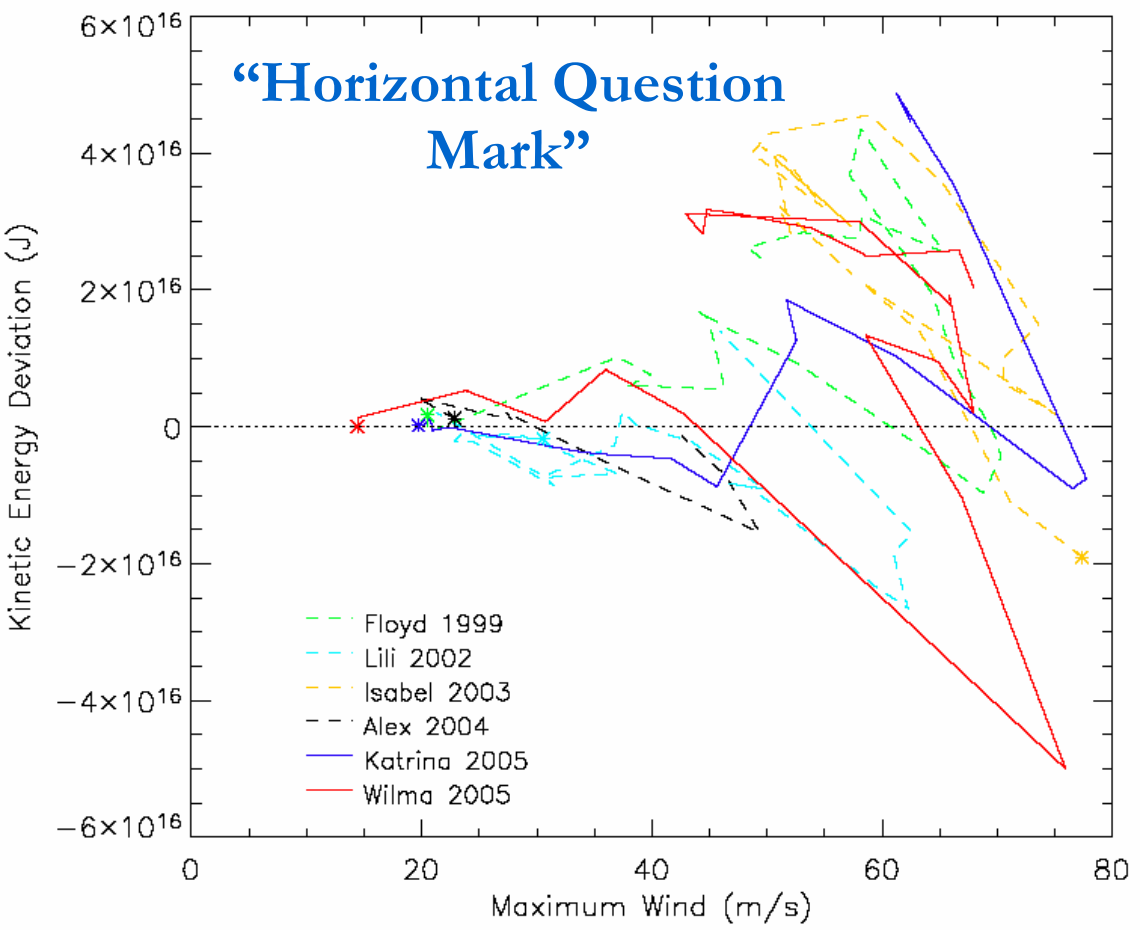

Figure 4: Time evolution of KE' versus V_{max} for six selected storms. Note in particular the plots for hurricane's Katrina and Wilma.

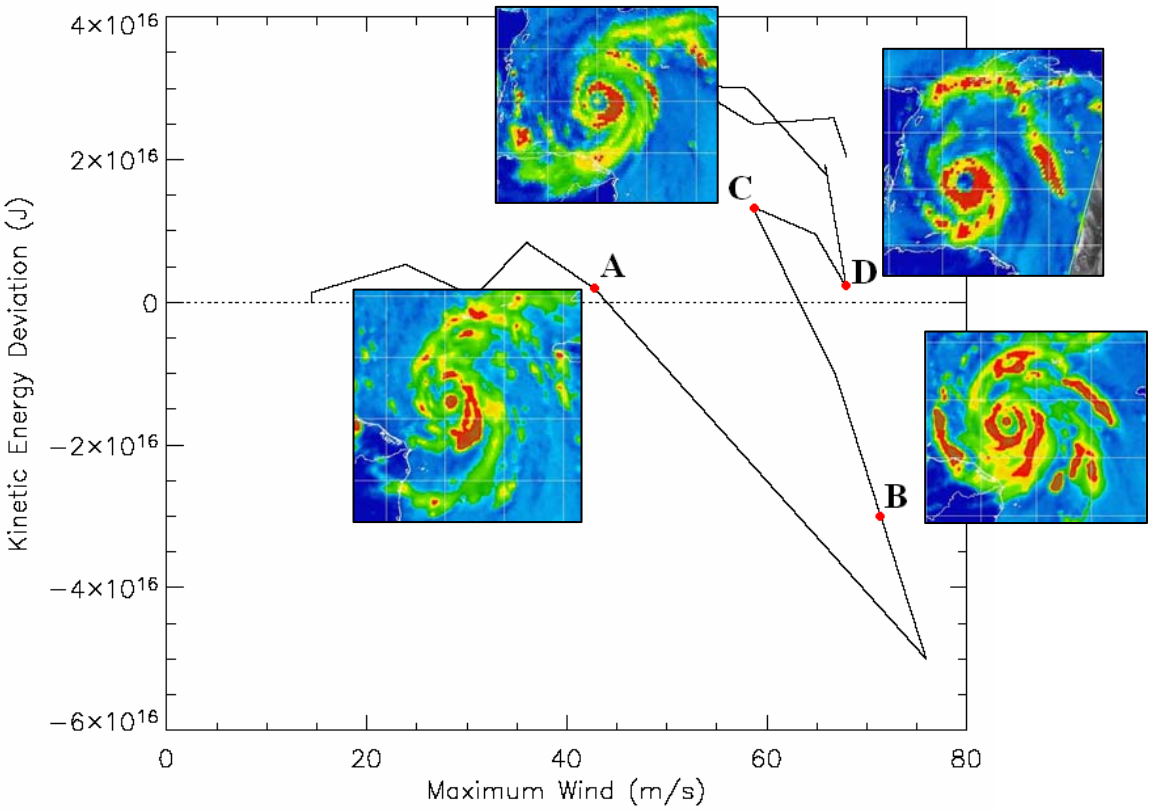

Figure 5: The KE' vs. V_{max} evolution of Hurricane Wilma with relevant microwave imagery overlain to illustrate the occurrence of an eyewall replacement cycle.

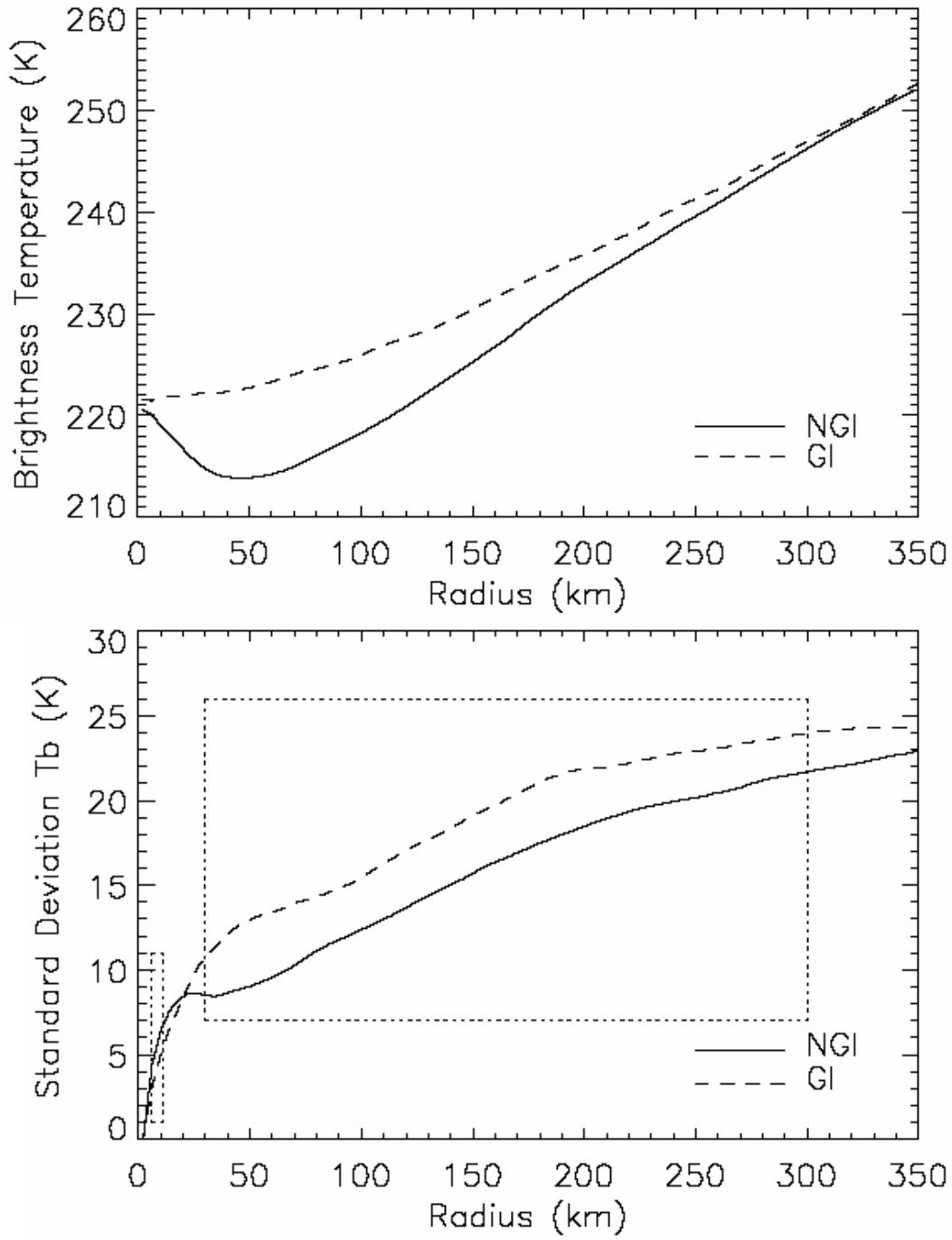

Figure 6: Mean radial profiles of the GOES IR brightness temperatures *(top*) and standard deviation in brightness temperatures (*bottom*) for intensifying storms. The boxes indicate the areas where the G versus NG storm profiles showed statistically significant differences.

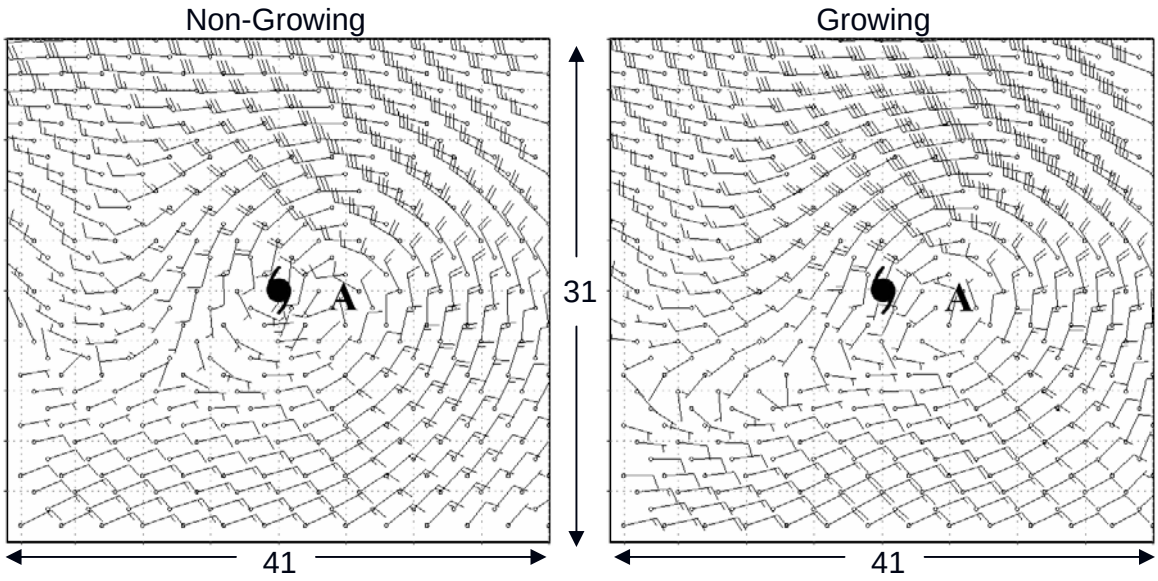

Figure 7: 200 hPa mean wind-fields [kts] for intensifying storms. The left-hand image shows the composite field for the non-growing storms, and the right-hand image shows the composite field for the growing storms. The cyclone symbol denotes the location of the center of the hurricane. The 'A' marks the location of the upper-level anticyclone.

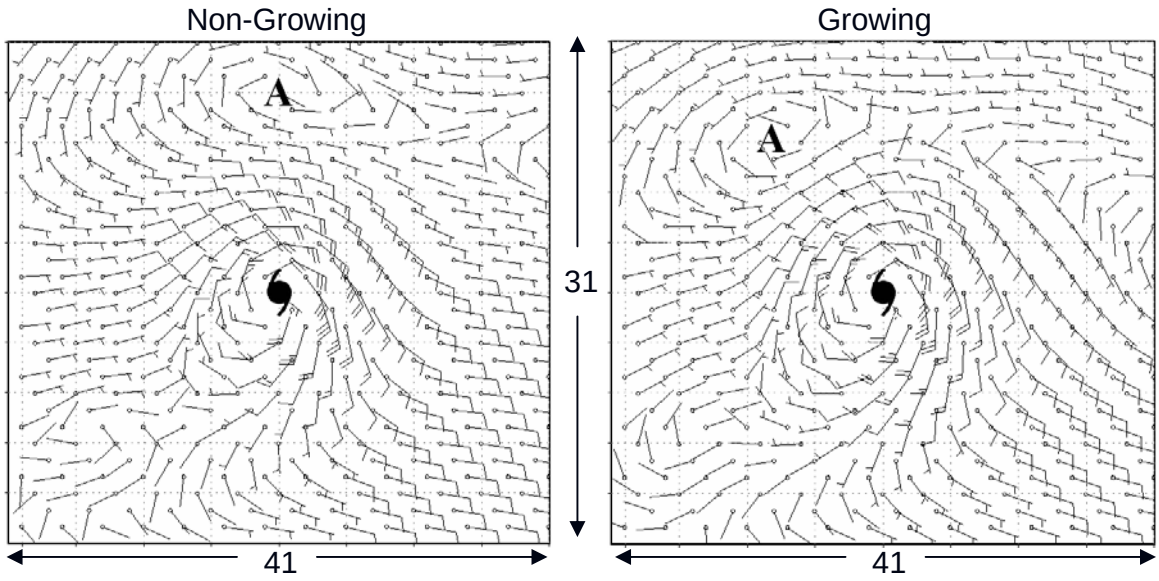

Figure 8: 850 hPa mean wind-fields [kts] for intensifying storms. The left-hand image shows the composite field for the non-growing storms, and the right-hand image shows the field for the growing storms. The cyclone symbol denotes the location of the center of the hurricane. The 'A' marks the location of the anticyclone circulation associated with the North Atlantic subtropical ridge.

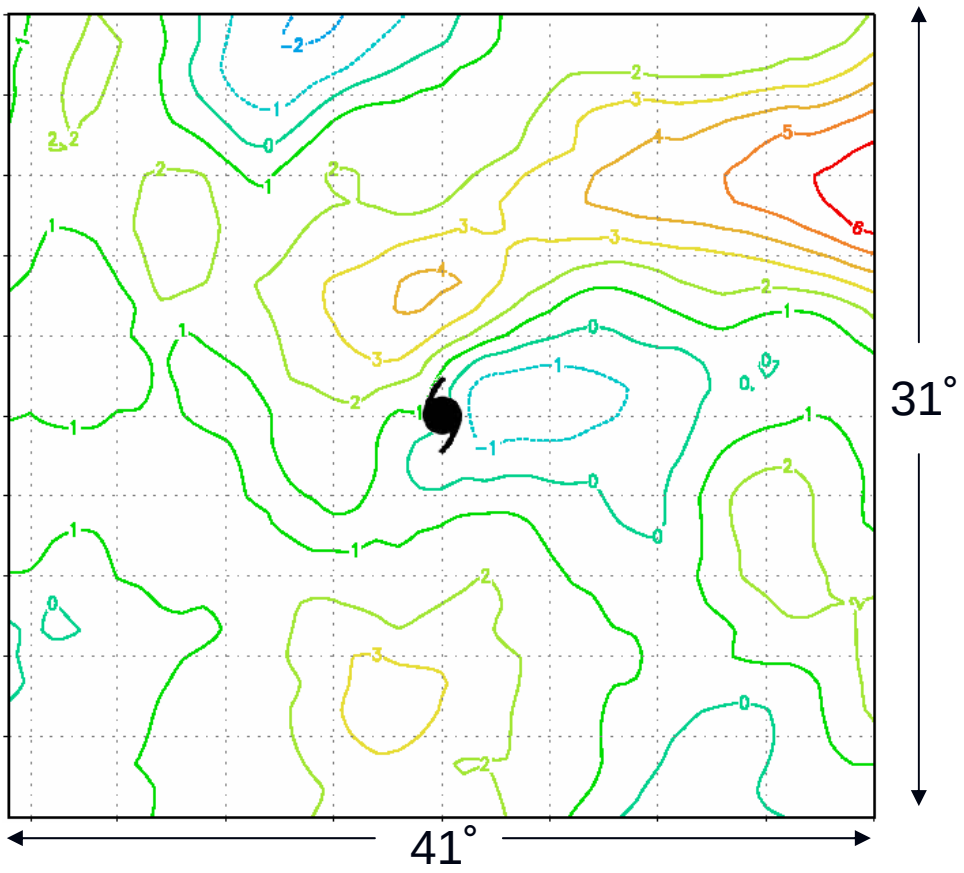

Figure 9: The difference in the mean 850-200 hPa shear [ms^{-1}] fields (growing – nongrowing) for intensifying storms. The cyclone symbol denotes the location of the center of the hurricane.

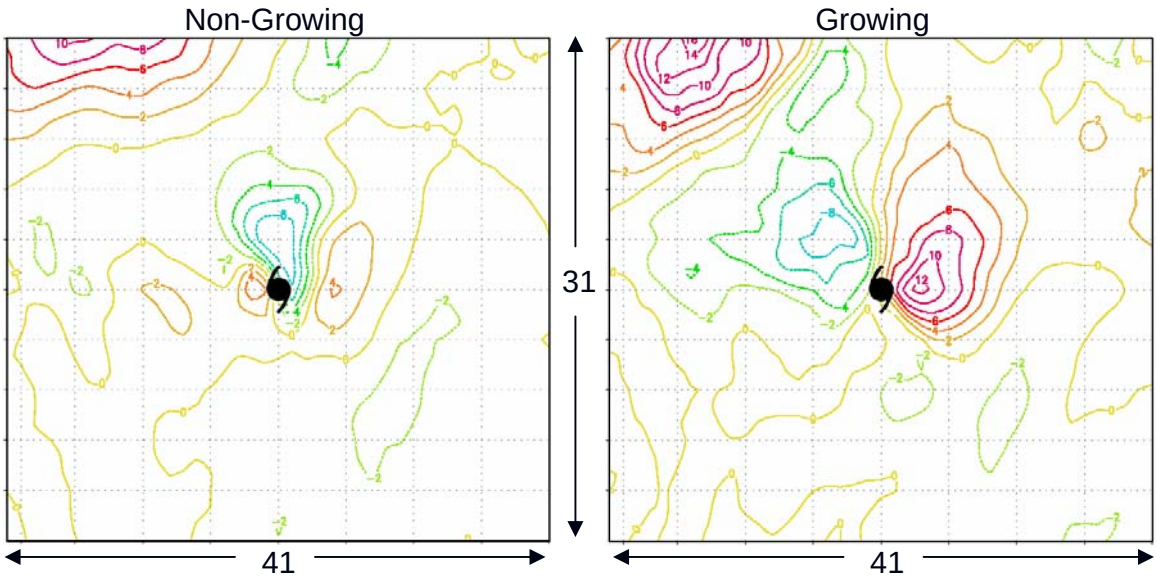

Figure 10: 700 hPa mean temperature advection [Ks^{-1}] fields for intensifying, non-growing (left) and growing (right) storms. The cyclone symbol denotes the location of the center of the hurricane.

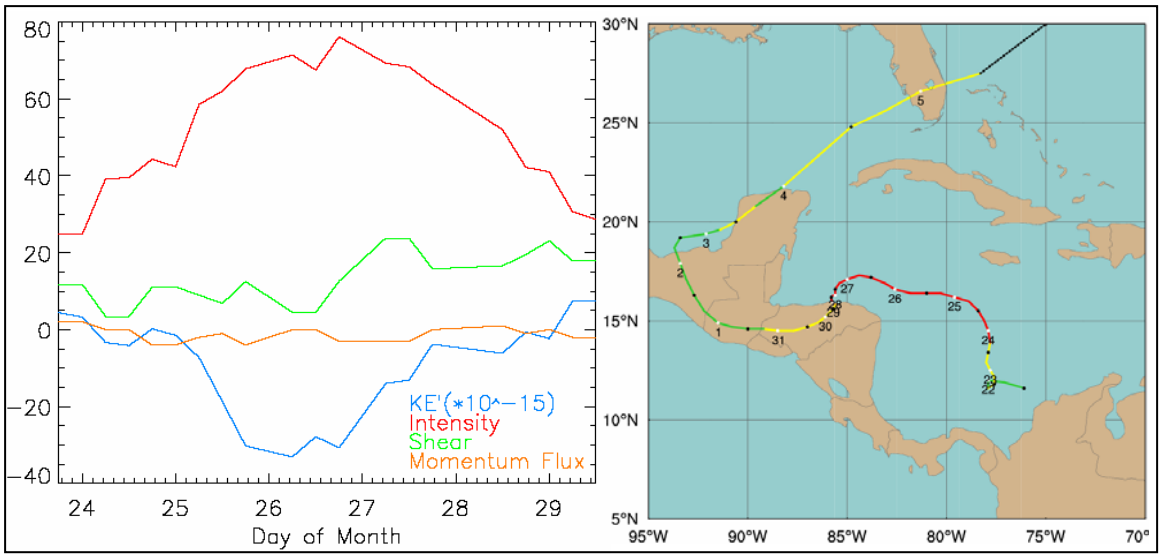

Figure 11: Time series of the intensity (ms^{-1}), environmental shear (ms^{-1}), 200 hPa eddy momentum flux convergence (ms^{-1} per day), and KE deviations (10^{16} J) from the mean curve for Hurricane Mitch (1998) (*left*); and the storm's track through its entire lifetime from NHC best-track (*right*). The time series plot corresponds to the storm's track over the Caribbean Ocean. The colors indicate the storm's intensity and the numbered data points correspond to day of the month.

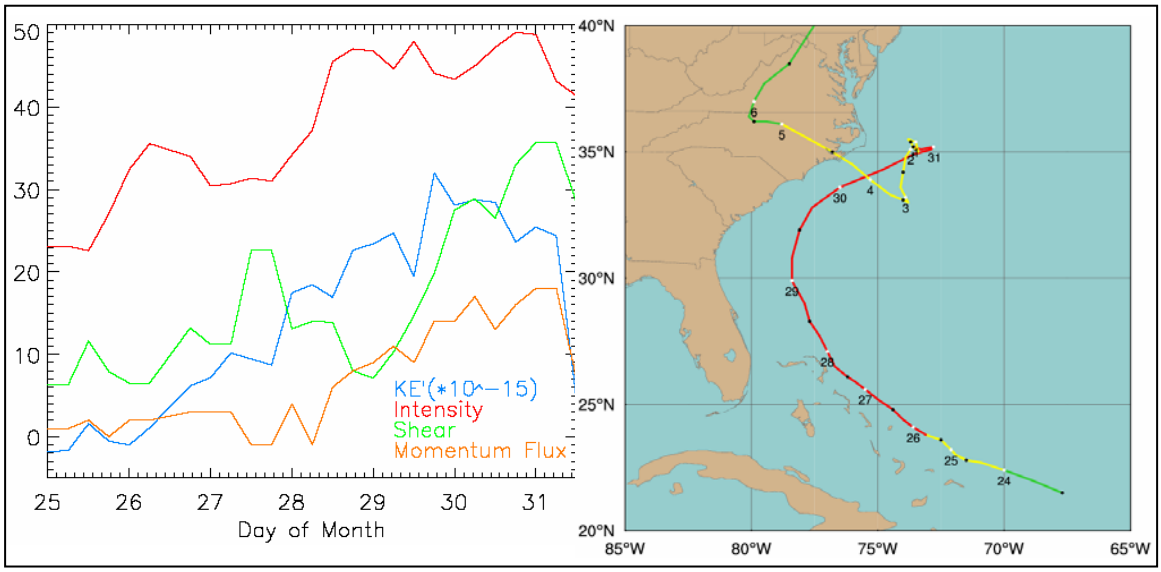

Figure 12: Time series of the intensity (ms^{-1}), environmental shear (ms^{-1}), 200 hPa eddy momentum flux convergence (ms^{-1} per day), and KE deviations (10^{16} J) from the mean curve for Hurricane Dennis (1999) (*left*); and the storm's track through its entire lifetime from NHC best-track (*right*). The colors indicate the storm's intensity and the numbered data points correspond to day of the month.

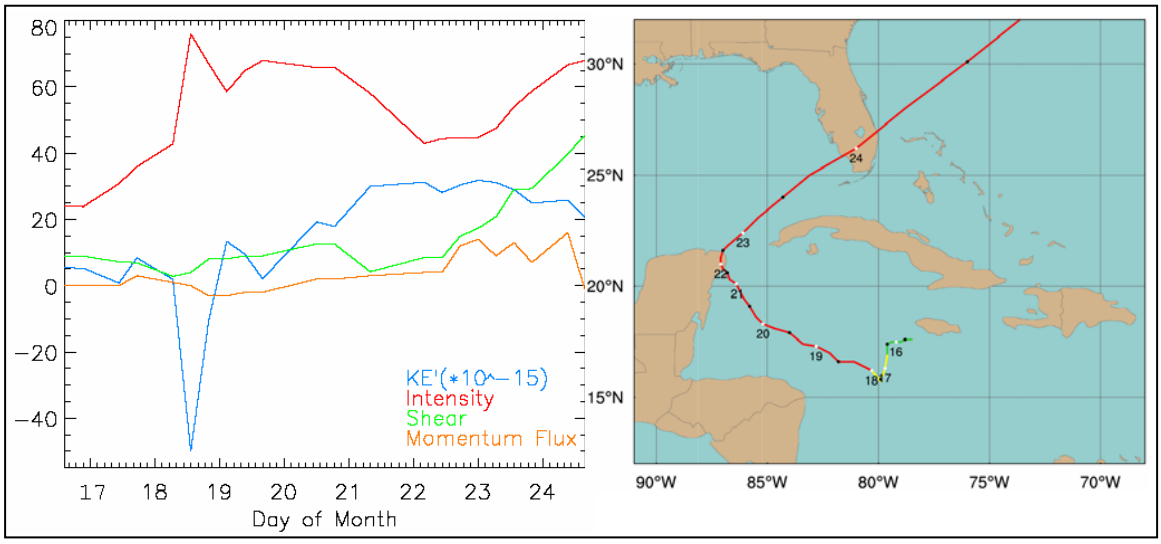

Figure 13: Time series of the intensity (ms^{-1}), environmental shear (ms^{-1}), 200 hPa eddy momentum flux convergence (ms^{-1} per day), and KE deviations (10^{16} J) from the mean curve for Hurricane Wilma (2005) (*left*); and the storm's track through its entire lifetime from NHC best-track (*right*). The colors indicate the storm's intensity and the numbered data points correspond to day of the month.